Numerical Simulation of Heat Transfer Problem in Hot and Cold Rolling Process

Ass.Prof. Dr. Ihsan Y. Hussain

Mech. Engr. Dept.
College of Engineering
University of Baghdad
Baghdad – Iraq

ABSTRACT

An efficient numerical model had been developed to model the thermal behaviour of the rolling process. An Eulerian formulation was employed to minimize the number of grid points required. The model is capable to calculate the temperature distribution, the heat penetration depth, the convection heat transfer coefficient of cooling, the flow of metal through the roll gap, and the heat generation by plastic deformation and friction. The roll is assumed to rotate at constant speed, and the temperature variations are assumed to be cyclically steady state and localized with a very thin layer near the surface. The Conventional Finite Difference (CFDM) based on cylindrical coordinates was used to model the roll, and a Generalized Finite Difference Method (GFDM) with non-orthogonal mesh was employed in the deformed strip region and the roll-strip interface area. An upwind differencing scheme was selected to overcome the numerical instability resulting from the high velocity (high Peclet number) involved in the rolling process. The equations of the strip and roll are then coupled together and solved simultaneously. Both cold and hot rolling heat transfer behaviours, velocity distribution, and heat generation by deformation and friction under typical rolling conditions were presented to demonstrate the feasibility and capability of the developed numerical model. It has been found that, while the strip is under deformation, the bulk temperature inside the strip increases continuously; this is largely controlled by the deformation energy. On the other hand, the strip surface temperature changes much more drastically and it is mainly controlled by the friction heat and the roll temperature. The roll acts like a heat sink, because the coolant heavily cools it. Thus, as soon as the strip hits the roll its surface temperature drops. Since considerable friction and deformation heat are created along the interface and transferred from the neighboring sub-layer, the surface temperature picks up rapidly. Finally, the results of the temperature distribution for both cold and hot rolling and the heat generation by deformation and friction obtained from the present study were compared with previous published work to verify the validity of the numerical solution. Good acceptable agreements were obtained.

الخلاصة

تم التوصل إلى نمـوذج عددي لنمذجه التصرف الحراري لعمليه ألدرفلة (Rolling Process). استخدمت صيغه أويلر العددية (Eulerian Formulation) لتقليل عدد نقاط ألشبكه (Mesh) اللازمة للحل العددي. للنموذج العددي القابلية على حساب توزيع درجات الحرارة ، عمق انتشار الحرارة (Heat Penetration Depth)، معامل انتقال الحرارة لمائع التبريد (Cooling Heat Transfer Coefficient)، جريان المعدن خلال عمليه الدرفلة (Flow of Metal in Rolling)، الحرارة المتولدة بسبب التشوه اللدن للمعدن (Heat Generation by Plastic Deformation and Friction). تم افتراض ثبوت السرعة الدورانيه للدرفيل وان التغيرات التي تطرأ على درجات الحرارة تكون على هيئه قشرة رقيقه (Very Thin Layer) على سطح الدرفيل. طريقة للفروقات المحددة التقليدية (Conventional Finite Difference Method) المبنية على أساس الإحداثيات القطبية (Polar Coordinates) هي الأكثر ملائمة والتي استخدمت لإيجاد توزيع درجات الحرارة للدرفيل. بينما استخدمت طريقة الفرو قات المحددة المعمّمة(Generalized Finite Difference Method) لنمذجة درجات الحرارة للمناطق التي تكون فيها خطوط الشبكه غير متعامدة (Non-orthogonal Mesh) و المتمثلة بالمنطقة التي يتشوه فيها المعدن. لقد اختير نسق لفرو قات الصاعد للنقاط المواجهة للجريان (Up-wind Differencing Scheme) للتغلب على عدم الاستقراريه العددية الناتجة من السرع العالية أو عدد بكلت العالي (High Peclet Number) الذي تتضمنه عمليه الدرفلة. تم حل معادلتي المعدن المدرفل (Strip) والدرفيل (Roll) آنيا (Simultaneously). تمت دراسة حالتي الدرفلة على البارد وعلى الساخن معا، عرضت نتائج التصرف الحراري و توزيع السرع وتوزيع الحرارة المتولدة بالتشوه والاحتكاك بمقتضى الشروط الحدودية النموذجية لإيضاح اقدرة النموذج الذي تم التوصل اليه. وجد في الدراسه الحالية، أثناء تشوه المعدن (Strip)، أن مقدار درجه الحرارة في داخله تزداد بصوره مستمرة، وأن طاقة التشويه تسيطر عليها بصوره كبيره. من ناحية أخرى فأن درجه حرارة سطح المعدن تتغير بصوره أكثر أثاره والتي تكون طاقه الاحتكاك ودرجه الحرارة داخل الدرفيل تسيطرعليها بصوره رئيسيه. أن التبريد العالي الذي يتعرض له الدرفيل، سيكون له أثر كبير أشبه بالغور الحراري(Heat Sink). حيث عند اصطدام المعدن بالدرفيل فأن درجه حرارة سطح الدرفيل تهبط. بسبب حرارتي التشوه والاحتكاك اللتان تتشآن على طول سطح التلامس (Interface) أضافه إلى الحرارة المنتقلة من الطبقة المجاورة للمعدن المشوه فأن درجه حرارة سطح المعدن ترتفع بسرعة. أخيرا، نتائج توزيعات درجه الحرارة والحرارة

المتولدة بسبب التشوه والاحتكاك التي تم التوصل لها قورنت بنتائج عمل مسبق للتحقق من مدى صحة الحل العددي. لقد وجد توافق جيد من المقارنة بين النتائج المحسوبة من البحث الحالي والنتائج المحسوبة في عمل مسبق.

KEY WORDS: Thermal Behaviour, Hot and Cold Rolling , Roll and Strip, Velocity and Temperature Distribution

INTRODUCTION

The process of plastically deforming metal by passing it between rolls is known as Rolling, **(Dieter 1986).** It can be considered as one of the most important of manufacturing process. Numerous investigations, numerical, analytical, and experimental have been carried out on rolling. In hot or cold rolling the main objective is to decrease the thickness of the metal. Ordinarily little increase in width occurs, so that decreases in thickness will result in an increase in length. As predicted by **(Lahoti and Altan 1975)** the energy consumed in plastic deformation is transformed into heat while a small portion of the energy is used up in deforming the crystal structure in material. This heat generation coupled with heat transfer within the deforming material and to the environment gives a temperature distribution in the deformed peace. As mentioned by **(Karagiozis and Lenard 1988),** a (± 1) percent variation of the temperature may cause (10) percent change in strength, which in turn will cause significant change in roll loads. As well as, the adequate cooling of roll and the rolled products is of a considerable concern to rolls designers and operators. Improper or insufficient cooling not only can lead to shorten roll life, due to thermal stresses, but it can also significantly affect the shape or crown of the roll and result in buckled strips or bunted edges. Considerable work has been done on modeling of the thermal behavior of rolling process. (Johnson and Kudo 1960) used upper pound technique to predict the strip temperatures. **(Lahoti *et al.* 1998)** used a two-dimensional finite difference model to investigate the transient strip and a portion of the roll behavior. **(Sheppard and Wright 1980)** developed a finite difference technique to predict the temperature profile during the rolling of the aluminum slab**. (Zienkiewicz *et al.* 1981)** submitted a general formulation for coupled thermal flow of metal for extrusion and rolling by using finite element method. **(Patula 1981)** with an Eulerian formulation attained a steady state solution for a rotating roll subjected to prescribed surface heat input over one portion and convective cooling over an other portion of the circumference. **(Bryant and Heselton 1982)** based on the idea of "rotating line sources of heat" and the strip modeling based on the theory of heat conduction in a "semi infinite body" they found that the knowledge of heat transfer mechanisms in hot rolling was essential to the study of many areas of the process. **(Bryant and Chiu 1982)** derived a simple model for the cyclic temperature transient in hot rolling work rolls. **(Tseng 1984)** investigated both the cold and hot rolling of steel by considering the strip and roll together. (Tseng ***et al.*** 1990) developed an analytical model **(Forier integral technique)** to determine the temperature profiles of the roll and strip simultaneously**. (Remn 1998)** used the Laplace and inverse transform analytic technique to study the two dimensional unsteady thermal behavior of work rolls in rolling process. **(Chang 1998)** used Finite difference formulations in the rolling direction and analytical solutions were applied normal to this direction, making computational more efficient. The experimental work done by **(Karagiozis and Lenard 1988)** shows the dependence of the temperature distribution during hot rolling of a steel slab on the speed of rolling, reduction ratio and initial temperature were investigated.

The purpose of the present study is to effectively analyze the thermal behavior of rolling process for hot and cold rolling by considering the roll and strip simultaneously for two cases of rolling conditions (see **Table 1** and **Fig. 1**) by using a suitable numerical methods.

MATHEMATICAL FORMULATION

The mathematical formulations of the problem will be presented in this article. The following assumptions were made;

1. The strip and roll are long compared with the strip thickness therefore; axial heat conduction can be neglected.

2. The steady state conditions are considered for both strip and roll.

3. Since tremendous rolling pressure builds up in the interface then, the surface roughness became insignificant, and the film is very thin, on the order of micron, therefore, the thermal resistance of the film can be neglected.

4. The constant friction coefficient was assumed along the interface.

5. No increase in width, so that the vertical compression of the metal is translated into an elongation in the rolling direction.

Using an Eulerian description, the energy equation of the strip for a planer steady state problem as shown in **(Tseng 1984)** is;

$$u\frac{\partial T_s}{\partial x}+v\frac{\partial T_s}{\partial y}=\alpha_s\left(\frac{\partial^2 T_s}{\partial x^2}+\frac{\partial^2 T_s}{\partial y^2}\right)+q_d/\rho_s c_s \qquad (1)$$

where (u) and (v) are the velocity component in (x and y) directions respectively which should satisfy the equation of continuity, (α, ρ and c) are the thermal diffusivity, density and specific heat respectively, (q_d) is the rate of heat generation by deformation per unit volume and the subscript (s) refers to the strip properties.

With respect to a fixed Eulerian reference frame, the governing partial differential equation of the roll temperature (T_r) as shown in **(Tseng 1990)** is;

$$\frac{\omega}{\alpha_r}\frac{\partial T_r}{\partial \theta}=\frac{\partial^2 T_r}{\partial r^2}+\frac{1}{r}\frac{\partial T_r}{\partial r}+\frac{1}{r^2}\frac{\partial^2 T_r}{\partial \theta^2} \qquad (2)$$

where (r) and (θ) are the cylindrical coordinates; (ω) is the roll angular velocity; and the subscript (r) refers to the roll properties.

The concept of the thermal layer has also been applied to a numerical analysis by (Tseng 1984) and in the present study, it has been improved computational accuracy.

According to **(Tseng 1984),** (δ/R) can be found as a function of the Peclet number ($Pe=R^2\omega/\alpha_r$). Alternately, following **(Patula 1981),** showed that ($\delta/R\le 4.24/\sqrt{Pe}$), when ($\sqrt{Pe}$ >>***0***), a condition satisfied in most commercial strip rolling.

Based on a numerical study of **(Tseng 1984**) the;

$$\delta/R=7/\sqrt{Pe} \qquad (3)$$

is large enough for the present numerical model.

For rolling situations involving high speeds, the penetration would be significantly less where ($Pe=R^2\omega/\alpha_r$). Conversely, for lower rotational speeds, the penetration would be greater.

In the present study (second case) and as reported by (Tseng 1990), the mean film coefficient of the water-cooling spray is about (3.4 W/cm^2.^{o}C) over about 30 degrees of the roll circumference. The secondary cooling produced by water puddling varies from (0.28 to 0.85 W/cm^2.^{o}C) as shown in **Fig. 2**. The two peak squares represent the entry and exit cooling. Puddling covers the remaining area.

As well as for the first case, the convection heat transfer for water cooling spray varies from (0.85 W/cm^2.^{o}C to 3.4 W/cm^2.^{o}C) along the roll. The heat transfers coefficient as presented in Fig. (4) varies as half sine curve to simulate both the entry and exit cooling. Then, from **Fig.3**. the heat transfer coefficient can be written as;

$$H(\theta) = 0.85 + 2.55\left|\sin(\theta)\right| \qquad \textbf{(4)}$$

Then, the two cases of water-cooling spray, **Figs. 2** and **3** are considered in the present study to simulate the entry and exit cooling during the rolling.

The flow of metal under the arc of contact is determined by assuming that the volume flow rate through any vertical section is constant. A metal strip with a thickness (t_o) enters the bite at the entrance plane (XX) with velocity (u_o). It passes through the bite and leaves the exit plane (YY) with a reduction thickness (t_f) and velocity (u_f) as shown in **Fig. 4**.

Since equal volumes of metal must pass at any vertical section, then;

$$Wt_o u_o = Wtu = Wt_f u_f \qquad \textbf{(5)}$$

where (W) is the width of strip; (u) is the velocity at any thickness (t) intermediate between (t_o) and (t_f).

At only one point along the arc of contact between the roll and strip is the surface velocity of the roll (V_r) equal the velocity of the strip. This point is called the neutral point or no-slip point and indicated in **Fig. 4** by point (N).

If large back tension or heavy draught is applied, the neutral point shifts toward the exit plane and the metal will slip on the roll surface, this (back tension) condition is considered in the present study.

There are two components of velocity, one of these in (x) direction is denoted by (u) and the other in (y) direction is denoted by (v). Recall **eq**. *(5),* then;

$$Wt_o u_o = Wt_f u_f = \underbrace{Wtu = Wt_n V_r} \qquad \textbf{(6)}$$

Thus;

$$u = \frac{t_n}{t} V_r \qquad \textbf{(7)}$$

When the equation of continuity is satisfied, then;

$$\frac{\partial u}{\partial x} + \frac{\partial v}{\partial y} = 0 \qquad \textbf{(8)}$$

Substitute eq. ***(7)*** in **eq. *(8),*** thus;

$$\frac{\partial}{\partial x}\left(\frac{t_n}{t}V_r\right)+\frac{\partial v}{\partial y}=0 \qquad \textbf{(9)}$$

After some arrangement the **eq.** ***(9)*** gives;

$$dv=\frac{t_n}{t^2}V_r\,\frac{dt}{dx}\,dy \qquad \textbf{(10)}$$

After integration **eq.** ***(10)*** becomes;

$$v=\frac{t_n}{t^2}V_r\,\frac{dt}{dx}\,y \qquad \textbf{(11)}$$

where (dt/dx) is the slope of the arc of contact at any (x).

In the present study for the second case, the deformation heat is distributed in the strip in proportion to the local effective strain rate and same as that distributed in **(Tseng 1984);**

$$\varepsilon_{eff}=\sqrt{(\varepsilon_x)^2+(\varepsilon_y)^2} \qquad \textbf{(12)}$$

Or;

$$\varepsilon_{eff}=\sqrt{\left(\frac{\partial u}{\partial x}\right)^2+\left(\frac{\partial v}{\partial h}\right)^2} \qquad \textbf{(13)}$$

In general, the deformation heat is proportional to both the strain rate and the flow stress, then;

$$Q_d \propto \varepsilon_{eff}\sigma_s)_{flow} \qquad \textbf{(14)}$$

where (Q_d) is the deformation heat generation (Kw); (ε_{eff}) is the strip effective strain rate (1/s) and (σ_S)$_{flow}$) is the strip flow stress (N/cm^2).

The distribution assumed in **eq.** ***(14)*** implies that the flow stress variation is small compared with very large strain rate as predicted by (Zienkiewicz *et al.* 1981) and **(Tseng 1984),** then;

$$Q_d \propto \varepsilon_{eff} \qquad \textbf{(15)}$$

Substitute **eq.** ***(8)*** with (y=h) and ***(7)*** in **eq.** ***(13)***, then;

$$\varepsilon_{eff}=\sqrt{2}\,\frac{\partial}{\partial x}\left(\frac{h_n}{h}V_r\right) \qquad \textbf{(16)}$$

After differentiation the **eq.** ***(16)***, then;

$$\varepsilon_{eff}=-\sqrt{2}\,\frac{h_n}{h^2}V_r\,\frac{dh}{dx} \qquad \textbf{(17)}$$

where (h_n) is the half thickness of the strip at the neutral point.

In the present study for the second case, the friction heat is distributed along the interface in proportion to the magnitude of the slip (relative velocity) between the roll and the strip as shown in **Fig**. **5**, then;

$$Q_{fr} \propto V_{slip} \qquad \textbf{(18)}$$

where (Q_{fr}) is the heat generation by friction (kW).

It is well known from **Fig. 8** that the slip velocity is;

$$V_{slip} = \left| V_r - \sqrt{u^2 + v^2} \right| \qquad \textbf{(19)}$$

As well as, the heat generated by deformation and friction for the first case study is assumed to be uniformly distributed in the bite and interface.

The input data of the heat generation by deformation and friction will be obtained from direct measurement of the power (**Table 1**) and it is considered in the present study.

As shown by **(Tseng 1984),** before entering and after exit the strip into and from the roll bite, the strip loses heat to the coolant by convection, see **Fig. 6**, then;

$$-k_s \frac{\partial T_s}{\partial n} = H_\infty (T_s - T_\infty) \qquad \textbf{(20)}$$

In the present study and in **(Dieter 1986 and Tseng 1984),** since the strip velocity is high, the conduction term, ($\partial^2 T_s / \partial x^2$) becomes small in comparison with the convection term, ($u \partial T_s / \partial x$). Thus the billet temperature should be the initial strip temperature (T_o).

The boundary condition as shown by **(Tseng 1984)** at some distance downstream from the exit contact point may be assumed to be;

$$\partial T_s / \partial x = 0 \qquad \textbf{(21)}$$

As showed by **(Tseng 1984)** because of the symmetry, the lower horizontal boundary having;

$$\partial T_s / \partial y = 0 \qquad \textbf{(22)}$$

The boundary condition for the roll circumference is;

$$-k_r \frac{\partial T_r(R,\theta)}{\partial r} = H(\theta)\{T_r(R,\theta) - T_\infty\} \qquad \textbf{(23)}$$

where ($H(\theta)$) is the heat transfer coefficient explained previously.

Since the roll is rotate rapidly, and all temperatures vary within a very thin layer near the surface, only a thin layer needs to be modeled. The interior boundary condition as shown by **(Tseng 1984)** becomes;

$$\partial T_r\left((R-\delta),\theta\right)/\partial r = 0 \qquad \textbf{(24)}$$

The strip is assumed to be in contact the roll and each moves relative to the other, creating the friction heat along the interface. Mathematically, as shown by **(Tseng 1984)** this boundary condition may be expressed as;

$$k_s\left(\frac{\partial T_s}{\partial n}\right)_b + k_r\left(\frac{\partial T_r}{\partial n}\right)_b - q_{fr} = 0 \qquad \textbf{(25)}$$

where ($\partial/\partial n$) represents differentiation along the normal of the boundary (positive outward); see **Fig. 9**; and (q_{fr}) is the friction heat generated along the interface and the subscript (b) refers to the boundary. All special derivatives for the points at the interface must be formulated using points located in their respective sides as follows;

$$k_s\left(\frac{\partial T_s}{\partial n}\right)_b = q_1 + q_2 \qquad \textbf{(26)}$$

Then, from **Fig. 7**;

$$\sin\beta_o = \frac{q_2}{k_s\left(\frac{\partial T_s}{\partial y}\right)_b},\ \cos\beta_o = \frac{q_1}{k_s\left(\frac{\partial T_s}{\partial x}\right)_b} \qquad \textbf{(27)}$$

Substituting **eq. *(27)*** in **eq. *(26)***, thus;

$$k_s\left(\frac{\partial T_s}{\partial n}\right)_b = k_s\left(\frac{\partial T_s}{\partial x}\right)_b \cos\beta_o + k_s\left(\frac{\partial T_s}{\partial y}\right)_b \sin\beta_o \qquad \textbf{(28)}$$

where the angle (β_o) specifies the direction as shown in **Fig. 7.**

Because the two bodies are in intimate contact, temperature equality at the interface is also assumed;

$$\left(T_s\right)_b = \left(T_r\right)_b \qquad \textbf{(29)}$$

Replacing $\left(\partial T_s/\partial n\right)_b$ by the directional derivatives **eq. *(28)*** and $\left(\partial T_r/\partial n\right)_b$ by $\left(\partial T_r/\partial r\right)_b$ and from **Fig. 7**, **eq. *(25)*** becomes;

$$\left(\frac{\partial T_s}{\partial x}\right)_b \cos\beta_o + \left(\frac{\partial T_s}{\partial y}\right)_b \sin\beta_o + \frac{k_r}{k_s}\left(\frac{\partial T_r}{\partial r}\right)_b - \frac{q_{fr}}{k_s} = 0 \qquad \textbf{(30)}$$

`NUMERICAL SOLUTION

In this article, the task of constructing the numerical method for solving the governing partial differential **eqs. *(1)*** and ***(2)*.**

The essence of GFDM is its ability to obtain the needed derivative expression at a given point as a function of arbitrarily located neighboring points. As reported by **(Tseng 1984)** for any sufficiently differentiable function, *T(x,y)*, in a given domain has Taylor series expansion about a point (x_o,y_o) up to second order terms can be written as;

$$T_{si} = T_{so} + m_i\left(\frac{\partial T_s}{\partial x}\right)_o + n_i\left(\frac{\partial T_s}{\partial y}\right)_o + \frac{m_i^2}{2}\left(\frac{\partial^2 T_s}{\partial x^2}\right)_o + \frac{n_i^2}{2}\left(\frac{\partial^2 T_s}{\partial y^2}\right)_o + m_i n_i\left(\frac{\partial^2 T_s}{\partial x \partial y}\right)_o \qquad \textbf{(31)}$$

where ($T_i=T(x_i,y_i)$, $T_o=T(x_o,y_o)$, $m_i=x_i-x_o$)and ($n_i=y_i-y_o$). Five independent equations, similar to **eq.** *(31)*, can be obtained by using five arbitrarily located neighboring points (x_i,y_i), $i=1,\ldots,5$, as shown in **Fig. 8.**

If the first special derivatives ($\partial T_s/\partial x \ldots \partial^2 T_s/\partial x\partial y$) at point (x_o,y_o) can computed in terms of the functional values at five neighboring points, see **Fig. 8**. In matrix form, as mentioned in **(Tseng 1984);**

$$\begin{bmatrix} m_1 & n_1 & m_1^2/2 & n_1^2/2 & m_1n_1 \\ m_2 & n_2 & m_2^2/2 & n_2^2/2 & m_2n_2 \\ m_3 & n_3 & m_3^2/2 & n_3^2/2 & m_3n_3 \\ m_4 & n_4 & m_4^2/2 & n_4^2/2 & m_4n_4 \\ m_5 & n_5 & m_5^2/2 & n_5^2/2 & m_5n_5 \end{bmatrix} \begin{Bmatrix} \partial T_s/\partial x \\ \partial T_s/\partial y \\ \partial^2 T_s/\partial x^2 \\ \partial^2 T_s/\partial y^2 \\ \partial^2 T_s/\partial x\partial y \end{Bmatrix} = \begin{Bmatrix} T_{s1}-T_{so} \\ T_{s2}-T_{so} \\ T_{s3}-T_{so} \\ T_{s4}-T_{so} \\ T_{s5}-T_{so} \end{Bmatrix} \qquad \textbf{(32)}$$

Or;

$$[A_{i,j}]\{DT_{sj}\} = \{T_{si}-T_{so}\} \qquad i\ ,j=1,2,\ldots,5 \qquad \textbf{(33)}$$

Inverse of the matrix $[A_{i,j}]$ leads to;

$$\{DT_{si}\} = [B_{i,j}]\{T_{si}-T_{so}\} \qquad i\ ,j=1,2,\ldots,5 \qquad \textbf{(34)}$$

where $[B_{i,j}]$ is the inverse of $[A_{i,j}]$. Rearranging **eq. *(34)*,** then;

$$\{DT_{si}\} = [B_{i,j}]\{T_{sj}\} \qquad i=1,\ldots,5,\ j=0,\ldots,5 \qquad \textbf{(35)}$$

where;

$$B_{io} = -\sum_{j=1}^{5} B_{ij} \qquad \textbf{(36)}$$

Finally the special derivatives at point (x_o,y_o) can be found as reported by **(Tseng 1984)** as;

$$\left(\frac{\partial T_s}{\partial x}\right)_o = \sum_{j=o}^{5} B_{1j} \quad T_{s\,j} \tag{37a}$$

$$\left(\frac{\partial T_s}{\partial y}\right)_o = \sum_{j=o}^{5} B_{2\,j} \quad T_{s\,j} \tag{37b}$$

$$\left(\frac{\partial^2 T_s}{\partial x^2}\right)_o = \sum_{j=o}^{5} B_{3\,j} \quad T_{s\,j} \tag{37c}$$

$$\left(\frac{\partial^2 T_s}{\partial y^2}\right)_o = \sum_{j=o}^{5} B_{4\,j} \quad T_{s\,j} \tag{37d}$$

Substituting the **eqs.** ***(36), (37a), (37b), (37c)*** **and** ***(37d)*** in the strip governing **eq.** ***(1),*** an algebraic approximation for each internal point was as reported by **(Tseng 1984);**

$$T_{so} = \frac{q_d \big/ \rho_s c_s - \sum_{j=1}^{5} \left(u_o B_{1j} + v_o B_{2\,j} - \alpha_s\, B_{3\,j} - \alpha_s\, B_{4\,j}\right) T_{sj}}{u_o B_{1o} + v_o B_{2o} - \alpha_s \left(B_{3o} + B_{4o}\right)} \tag{38}$$

For the boundary points, spatial care is required. Substituting **eq.** ***(30)*** with $\left(\partial T_r / \partial r\right)_b = \left(\left(T_{ro} - T_r\right)/\Delta r\right)$ and ($\Delta r = r_o - r_j$) into **eq.** ***(31),*** from **eq.** ***(30)*** after the final substitution, eliminate $\left(\partial T_s / \partial x\right)_o$ or $\left(\partial T_s / \partial y\right)_o$. If ($\beta_o \neq 0$ or $\neq \pi$), keep $\left(\partial T_s / \partial x\right)_o$ and find;

$$T_{si} = \left(1 + a_1 n_i\right) T_{so} + \left(m_i + a_2 n_i\right)\left(\frac{\partial T_s}{\partial x}\right)_o + a_3 n_i + \frac{1}{2}\left(\frac{\partial^2 T_s}{\partial x^2}\right)_o m_i^2 + \frac{1}{2}\left(\frac{\partial^2 T_s}{\partial y^2}\right)_o n_i^2 + \left(\frac{\partial^2 T_s}{\partial x \partial y}\right)_o m_i n_i \tag{39}$$

where;

$$a_1 = \frac{k_r}{k_s \Delta r \sin \beta_o} \tag{40}$$

$$a_2 = -\cot \beta_o \tag{41}$$

$$a_3 = -\frac{1}{k_s \sin \beta_o}\left(\frac{k_r}{\Delta r} T_r + q_{fr}\right) \tag{42}$$

As reported by **(Tseng 1984),** upon providing four arbitrary selecting neighboring points, **Fig. 9**, four independent equations similar to **eq.** ***(39)*** can be obtained by following the procedure similar to that for treating the internal points, then;

$$[D_{ij}]\ \{DT_{sj}\} = \{f_i - T_{so}\} \qquad i, j = 1, \ldots\ldots, 4 \tag{43}$$

where;

$$D_{i1}=\frac{m_i+a_2 n_i}{1+a_1 n_i}\ , \qquad D_{i2}=\frac{m_i^2}{2(1+a_1 n_i)}\ , \qquad D_{i3}=\frac{n_i^2}{2(1+a_1 n_i)}$$

$$D_{i4}=\frac{m_i n_i}{1+a_1 n_i}\ , \qquad f_i=\frac{T_{si}-a_3 n_i}{1+a_1 n_i}$$

and $\{DT_{si}\}$ is column matrixes containing the four derivatives of **eq. *(39)*.**

Again, inversion of $[D_{ij}]$ leads to;

$$\{DT_{si}\}=[E_{ij}]\{f_j\} \qquad i=1,\ldots,4,\ j=0\ldots,\ 4 \qquad \textbf{(44)}$$

where $[E_{ij}]$ is the inverse of $[D_{ij}]$, $f_o=T_{so}$, and $E_{io}=-\sum_{j=1}^{4}E_{ij}$. Thus, the special derivatives at the boundary points, (x_o,y_o) become;

$$\left(\frac{\partial T_s}{\partial x}\right)_o=\sum_{j=0}^{4}E_{1j}f_j \qquad \textbf{(45a)}$$

$$\left(\frac{\partial^2 T_s}{\partial x^2}\right)_o=\sum_{j=0}^{4}E_{2j}f_j \qquad \textbf{(45b)}$$

And;

$$\left(\frac{\partial^2 T_s}{\partial y^2}\right)_o=\sum_{j=0}^{4}E_{3j}f_j \qquad \textbf{(45c)}$$

Substituting **eq. (45a)** in **eq. (28)** and determining $(\partial T_s/\partial y)_o$, then;

$$\left(\frac{\partial T_s}{\partial y}\right)_o=a_2\sum_{j=0}^{4}E_{1j}f_j+a_1 f_o+a_3 \qquad \textbf{(45d)}$$

Substituting the **eqs. *(45a), (45b), (45c)* and *(45d)*** into strip governing **eq. *(1),*** an algebraic relationship for the boundary point (x_o,y_o) was as reported by **(Tseng 1984);**

$$T_{so}=\frac{\sum_{j=1}^{4}\left[\alpha_s(E_{2j}+E_{3j})-(u_o+a_2 v_o)E_{1j}\right](T_{sj}-a_3 n_j)/(1+a_1 n_j)-a_3 v_o+q_d/\rho_s c_s}{(u_o+a_2 v_o)E_{1o}+a_1 v_o-\alpha_s(E_{2o}+E_{3o})} \qquad \textbf{(46)}$$

Upwind scheme was employed to achieve numerical stability, then;

$$T_{si} = T_{so} + m_i \left(\frac{\partial T_s}{\partial x} \right)_o + n_i \left(\frac{\partial T_s}{\partial y} \right)_o \qquad \textbf{(47)}$$

Two simultaneous equations were obtained by using two neighboring points (*1* and *2*). After rearranging these two equations into matrix form, then;

$$\left(\frac{\partial T_s}{\partial x} \right)_o = \sum_{j=0}^{2} F_{1j} T_{sj} \qquad \textbf{(48a)}$$

$$\left(\frac{\partial T_s}{\partial y} \right)_o = \sum_{j=0}^{2} F_{2j} T_{sj} \qquad \textbf{(48b)}$$

Substitute the **eqs.** ***(60a)*** and ***(60b),*** and those in **eqs.** ***(49c)*** and *(49d)* to the strip governing **eq.** ***(1),*** the first upwind GFDM equation for each internal point was as reported by **(Tseng 1984);**

$$T_{so} = \frac{q_d / \rho_s c_s - \sum_{j=1}^{2} \left(u_o F_{ij} + v_o F_{2j} - \alpha_s B_{3j} - \alpha_s B_{4j} \right) T_{sj} + \alpha_s \sum_{j=3}^{5} \left(B_{3j} + B_{4j} \right) T_{sj}}{u_o F_{1o} + v_o F_{2o} - \alpha_s \left(B_{3o} + B_{4o} \right)} \qquad \textbf{(49)}$$

For the typical boundary condition described in **eq.** ***(30),*** and using the same notations as in **eqs.** ***(39)*** and ***(43)*** for (a_i and f_j), respectively, point (*1*) is again to be an upwind point, **Fig. 9**, then;

$$T_{si} = \left(1 + a_1 n_i \right) T_{so} + \left(m_i + a_2 n_i \right) \left(\frac{\partial T_s}{\partial x} \right)_o + a_3 n_i + (all\ terms = 0) \qquad \textbf{(50)}$$

Or;

$$\left(\frac{\partial T}{\partial x} \right)_o = \sum_{j=0}^{1} G_j f_j \qquad \textbf{(51)}$$

And;

$$\left(\frac{\partial T}{\partial y} \right)_o = a_2 \sum_{j=0}^{1} G_j f_j + a_1 f_o + a_3 \qquad \textbf{(52)}$$

where $G_1 = -G_o = \left(1 + a_1 n_1 \right) / \left(m_1 + a_2 n_1 \right)$.

Substitute the **eqs.** ***(51), (52), (45b)*** and ***(45c)*** into strip governing **eq.** ***(1),*** an upwind GFDM relationship for a boundary point (x_o,y_o) was as reported by **(Tseng 1984);**

$$T_{so} = \frac{\alpha_s \sum_{j=1}^{4} \left(E_{2j} + E_{3j} \right) f_j - \left(u_o + a_2 v_o \right) G_1 f_1 - a_3 v_o + q_d / \rho_s c_s}{\left(u_o + a_2 v_o \right) G_o + a_1 v_o - \alpha_s \left(E_{2o} + E_{3o} \right)} \qquad \textbf{(53)}$$

The roll governing eq. ***(2)***, is approximated by using second order central differencing for the conduction terms (right side) and first order up wind differencing for the convection terms (left side).

The temperature profile becomes identical in a plot of normalized temperature, $T_r^* = H_o(T_r - T_\infty)/q_o$, against, $r^* = r/R$, which will certainly simplify further parametric study and high accuracy.

Then, in dimensionless form the roll governing **eq. *(2)*** becomes;

$$\frac{1}{r_o^*}\frac{\partial T_r^*}{\partial r^*} + \frac{1}{r_o^{*2}}\frac{\partial^2 T_r^*}{\partial \theta^2} + \frac{\partial^2 T_r^*}{\partial r^2} = Pe\frac{\partial T_r^*}{\partial \theta} \qquad \textbf{(54)}$$

where the superscript (*) refers to the dimensionless quantity.

By using four arbitrary located neighboring points as shown in **Fig.10**, then the roll governing eq. ***(2)*** becomes;

$$\frac{T_{r4}^* - 2T_{ro}^* + T_{r2}^*}{\Delta r^{*^2}} + \frac{1}{r_o^*}\frac{T_{r4}^* - T_{r2}^*}{2\Delta r^*} + \frac{1}{r_o^{*^2}}\frac{T_{r3}^* - 2T_{ro}^* + T_{r1}^*}{(2\Delta\theta)^2} = Pe\frac{T_{ro}^* - T_{r1}^*}{\Delta\theta} \qquad \textbf{(55)}$$

Rearranging the above equation, an algebraic approximation for roll internal nodes is;

$$T_{ro}^* = \left\{a_{r1}T_{r1}^* + a_{r2}T_{r2}^* + a_{r3}T_{r3}^* + a_{r4}T_{r4}^*\right\}/a_{ro} \qquad \textbf{(56)}$$

where;

$$a_{r1} = \frac{1}{(2r_o^*\Delta\theta)^2} + \frac{Pe}{\Delta\theta}, \qquad a_{r2} = \frac{1}{(\Delta r^*)^2} + \frac{1}{2r_o^*\Delta r^*}, \qquad a_{r3} = \frac{1}{(2r_o^*\Delta\theta)^2}$$

$$a_{r4} = \frac{1}{(\Delta r^*)^2} + \frac{1}{2r_o^*\Delta r^*}, \qquad a_{ro} = \frac{Pe}{\Delta\theta} + 2\left(\frac{1}{(2r_o^*\Delta\theta)^2} + \frac{1}{(\Delta r^*)^2}\right)$$

RESULTS AND DISCUSSION

This article presents the numerical results of the present work, besides, a verification of the computational model will also be made.

Fig. 11 show the horizontal component of velocity for the first case study. In the billet region, the strip has velocity (u) only, i.e., (v=0). Since equal volumes of metal must pass at any vertical section through the roll gap and the vertical elements remain undistorted (no increase in width), **eq. *(13)*** requires that the exit velocity must be greater than entrance velocity, therefore, the velocity (u) of the strip must be steadily increased from entrance to exit. the exit product region having (u) velocity only, i.e., (v=0).

The vertical component of velocity (v) for the first case study and for different lines are shown in **Fig.12**. In the billet, the streamlines are horizontal and having horizontal component of velocity (u) only and (v=0). After entering the bite the streamlines have curved shapes and the slopes of these curves gradually decrease from entrance to exit. Then the velocity (v) gradually diminishes from entrance to exit as shown in **eq. *(11)*** and in **Figs.12**. The horizontal and vertical

components of the velocity for the second case study are similar to those in the first case but the different in the elevations

As mentioned by many authors such as **(Tseng 1984)** and **(Lahoti *et al.* 1978),** rolling a mild steel as shown in **Table 1,** consume about (90) percent of the total power in the deformation of the strip and in the friction loss at the interface. Moreover, according to **(Zienkiewicz *et al.* 1981)** and **(Tseng 1984)** who measured both the plastic work and the temperature rise in a tensile experiment. It was found that for steels, copper and aluminum, the heat rise represents (86.5, 90.5-92 and 95) percent, respectively, of the deformation energy which is converted into heat.

In the present study, this (90) percent estimated is used, i.e., that (6.5) percent of (90) percent of total power is dissipated as friction heat along the interface.

The resulting values of the heat generation by deformation and friction were summarized in the **Table 2** for the first and second case study. In the first case, the heat generation by deformation and friction are distributed. In the second case, the heat generation by deformation is then distributed to the strip in proportion to the local effective strain rate as shown in **eqs. *(15)*** and ***(17)*** and **Fig.13**. Note that the highest strip deformation (strain rate) occurs near the bite entry and diminishes monotonically toward the end of the bite as shown in **Fig.13.** Thus, the highest heat generation by deformation occurs near the bite entry too and diminishes monotonically toward the end of the bite as shown in **eq. *(19)*** and **Fig. 13.**

Also, the strip is to be moved relative to the roll creating friction heat along the interface as recorded in **eq. *(19),*** i.e., the friction heat is then distributed in proportion to the (relative velocity between the strip and roll as recorded in **eq. *(18)*** and in **Fig.14**. The maximum slip occurs at the first point of contact at the interface because the roll draws the thick strip into the bite. Then, the slip velocity decreases gradually until sticking at the final point of contact as shown in **Fig. 14.**

Figs.15 and **16**, indicate that the roll temperature variations are limited within a very thin layer, about (1) percent of the radius, which consistent with the associated boundary condition eq. ***(24)***. The surface temperature rapidly increases at the bite due to great heat generated by the friction and transferred from the strip. As the roll leaves the bite, the roll surface temperature immediately decreases due to heat convected to the coolant and heat conducted into the immediate sub surface layer.

As well as, as shown in **Figs. 15** and **16** the different in temperatures between the final and initial points of contact for the first case study is less than for the second case. This means, using several small coolant sprays (second case) is more efficient than one large spray (first case).

Figs. 17 and **18** indicate that while the strip is under deformation, the bulk temperatures inside the strip increase continuously; this is largely controlled by the deformation energy. On the other hand, the strip surface temperature changes much more drastically and it is mainly controlled by the friction heat and the roll temperature.

The coolant heavily cools the roll; it acts like a heat sink. Thus, as soon as the strip hits the roll its surface temperature drops as shown in **Figs. 17** and **18**. Since considerable friction and deformation heat are created along the interface and transferred from the neighboring sub layer, the surface temperature picks up rapidly.

Beyond the bite, **Figs.17** and **18**, the strip temperature tends to be uniform. In this region, the heat convected to the air has been assumed to be negligible. For high-speed rolling (rather than the considered limits), the product temperature behaves parabolically rather than elliptically as implied by **eq. *(1)*.** In other words, the boundary conditions that are assumed in the product should not have a noticeable effect on the bite region.

The interface heat fluxes results for uniform and non-uniform heat generation distributions are shown in **Figs.19** and **20**. At the initial contact stage, as anticipated, a very large amount of heat is transferred to the roll. In fact, the roll surface temperature is about (25 ^{o}C and 11.0362 ^{o}C) lower than that of the strip as shown in **Figs. 15, 16, 17** and **18.**

To satisfy the boundary condition **eq. *(29),*** a step change of surface temperatures are expected to occur at the initial contact point ($x=0$). The induced heat flux to the roll at (x=0) as

shown in **Figs. 19** and **20**, also ensure the above findings that a large amount of heat is transferred to the roll from strip and the interface friction at the initial contact stage.

It is believed that in the previous studies, the strip initial temperatures were close to that of the roll. Therefore, the strip is not expected to have a temperature drop at the initial contact stage. However, it is note worthy that at very high rolling speeds, measuring the local temperature change in the bite could be a big challenge as mentioned previously in **(Tseng 1984).**

In hot rolling, the strip is normally rolled at elevated temperatures at which re-crystallization proceeds faster than work hardening. In addition, the hot strip is generally rolled at thicker gages and lower speed than that of the cold strip.

The gages specified in the first case are still suitable for hot rolling. Two focuses are considered. The first focuses on the effect of changing the entering temperature to (900 ^{o}C). The second, changing velocity by slowing the roll speed from (1146.6 to 573.3 cm/s). The other operating conditions are similar to those discussed for cold rolling.

Fig. 21 depicts the roll temperature distribution for the two hot rolling cases consider (V_r=1146.6 and 573.3 cm/s). A comparison of **Fig.21** with **Fig.17** indicates that the temperature profile between the hot and cold rolling is mainly in magnitude but not in shape.

Both the interface heat flux and speed govern the temperature magnitude. As shown in **Fig. 22** at speed of (1146.6 cm/s), the heat flux increases about four times for the hot to cold rolling. The corresponding increase of temperature is also found to be about four times too as shown in **Fig. 21.**

Fig. 21 shows except in the bite region, the roll temperature is reducing about (15) percent with the speed slowed to (50) percent, and the different in the bite region is much smaller and the maximum temperature occurs at the end the arc of contact. For example, the corresponding decrease of the peak temperature is less than (2) percent. The temperature decrease due to slowing the speed is mainly due to decrease of the heat flux **Fig. 22**.

Figs. 21 and **23** also show that near the bite, very large temperature variations are within a very thin layer. The layer thickness (δ), consistent with the previous finding, is dependent on the speed, or more precisely, the roll Peclet number as shown in **eq. *(3)*.**

The strip temperatures for the two hot rolling cases are presented in **Fig. 24**. In the bite region, the strip temperature, similar to the roll temperatures, is not noticeably affected by changing the speed within the range consider. In the down stream region ($x>x_o$), the strip center temperature drops faster in the slower strip. By contrast, the surface temperatures are not sensitive to the speeds considered. This figure also indicates the temperature drop in the initial contact stage is much large than its counterpart for the clod strip, as shown in **Fig. 24**. When the strip entry temperature rises from (65.6 ^{o}C) to (900 ^{o}C) from cold to hot rolling, the temperature drop increases approximately from (25 ^{o}C) to (649 ^{o}C), reflecting the great increase in the temperature different between the strip and roll a head of the bite.

The shape of the heat input distribution to the roll (q_r) governs the roll and strip temperatures in the roll gap region. As shown in **Figs.18** and **23** with a parabolic distribution of (q_r) of the second case study, the location of the maximum temperature shifts to the interior of the arc of contact (heating zone). Although, the cumulative energy input is still increasing beyond ($\Phi/2$), the flux is decreasing, yet the effect of the type of heat distribution on the temperature distribution away from the roll gap should be minimal as shown in **Figs 21** and **23.**

CONCLUDING REMARKS

1. While the heat generation by deformation occurs in the strip or by friction at the strip-roll interface and the heat removal is at the roll surface, then, both strip and roll should be considered together and solved simultaneously.

2. The highest heat generation by the deformation and friction occurs at the entrance to the bite and diminishes gradually toward the end of the bite.

3. The results show that the extremely large temperature drop at the interface and large temperature variation in both roll and strip are found. Such high temperature variations could

create very large (δ) thermal stresses within the thin layer and this stresses lead to the roll wear or roll failure, then proper control of this stresses could significantly extend the roll life.

4. Several small coolant sprays (second case) are more efficient than one large spray (first case).

5. The temperature decreases due to slowing the roll speed. This is mainly due to decrease the total input power that led to decrease of the heat flux at the interface.

6. The shape of the heat input distribution (uniform or parabolic heat input) to the roll governs the location of the peak temperature.

Finally, the comparison of the present results with published findings by (Tseng 1984) shows that the computational scheme used is effective and reliable. However, it is believed that the greatest uncertainty in analysis will arise not from the numerical scheme, but from the input data, in particular, the friction energy, the location of the neutral point (or the forward slip), and the heat transfer coefficient of coolant.

Table 1 : Operational Parameters for the First and Second Case Studies.

Operational Parameters	First Case, for Coil 45, Tseng 1984.	Second Case, for Coil 32, Tseng 1984
Strip Material.	Mild Steel.	Mild Steel.
Roll Material.	Cast Steel.	Cast Steel.
Coolant.	Water.	Water.
Entry Gauge.	0.15 cm.	0.085 cm.
Exit Gauge.	0.114 cm.	0.057 cm.
Roll Speed.	1146.6 cm/s.	1219 cm/s.
Forward Slip.	0	0
Strip Width.	63.5 cm.	81.3 cm.
Roll Diameter.	50.8 cm.	50.8 cm.
Total Input Energy.	3694 kW.	3340 kW.
Strip Entry Temperature.	65.6 ^{o}C.	65.6 ^{o}C.

Both the roll and the strip have the following thermal properties: -

Thermal conductivity (k_r, k_s); 0 .4578 W/cm.^{o}C

Thermal diffusivity (α_r ,α_s); 0.1267 cm^2/s

Table 2 : Amounts of the Heat Generation by Deformation and Friction.

Case Number	Heat Generation by Plastic Deformation Q_d (kW)	Heat Generation by Friction Q_{fr} (kW)
١st	٢٤٥٠	١٩٨
٢nd	٢٦٨٩	٢١٧

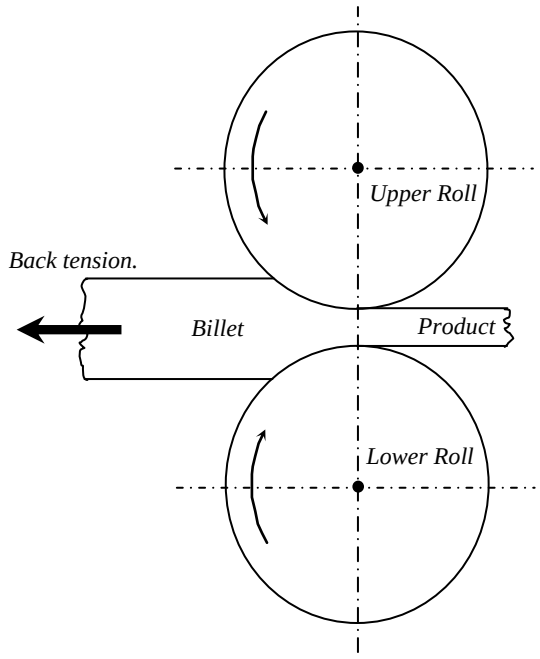

Fig. 1: Typical Arrangement of Rolls for Rolling Process.

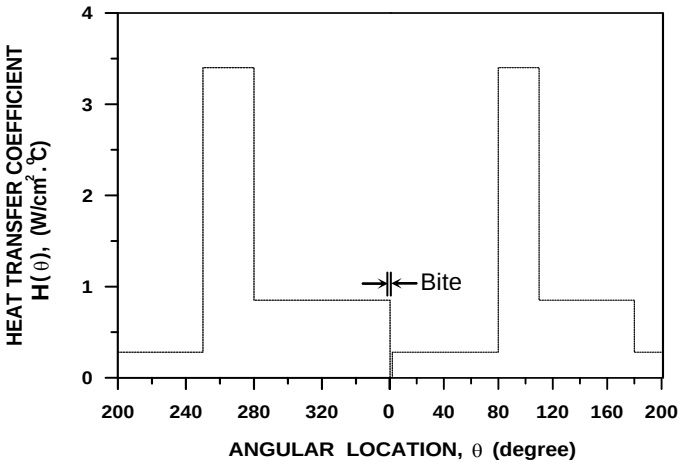

Fig. 2: Cooling Heat Transfer Coefficient, Tseng 1984

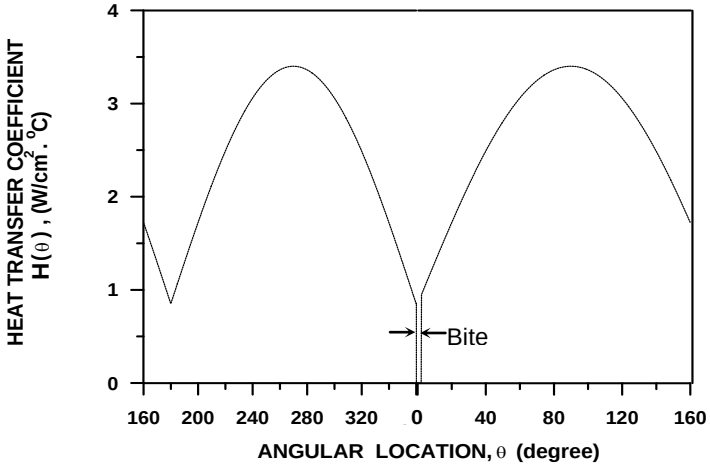

Fig. 3: Heat Transfer Coefficient that Varies as A Half Sine Curve,Patula 1981

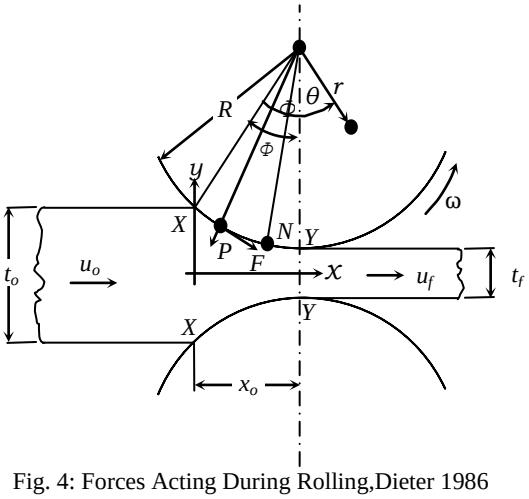

Fig. 4: Forces Acting During Rolling,Dieter 1986

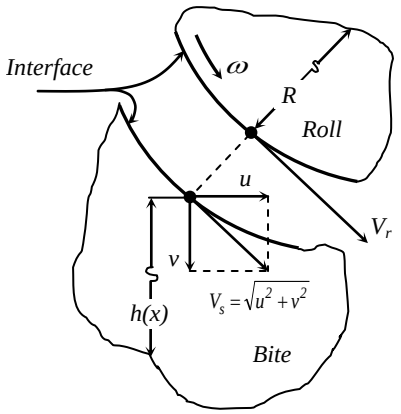

Fig. 5: The Relative Velocity between the Roll and Strip.

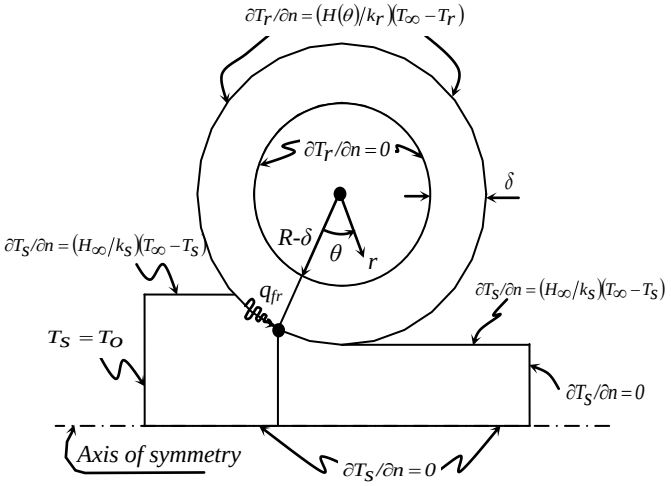

Fig. 6: Typical Boundary Conditions for Strip, Roll and Interface Region, Tseng 1984

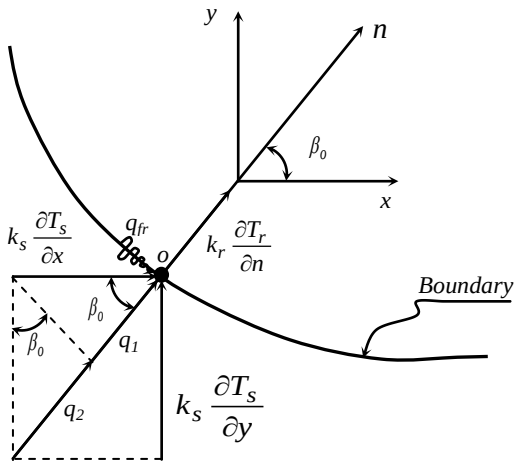

Fig. 7: The Components of Interface Heat Flux.

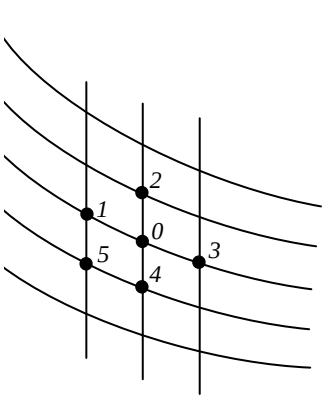

Fig. 8: The Grid Arrangement for the Strip Internal Nodes, Tseng 1984

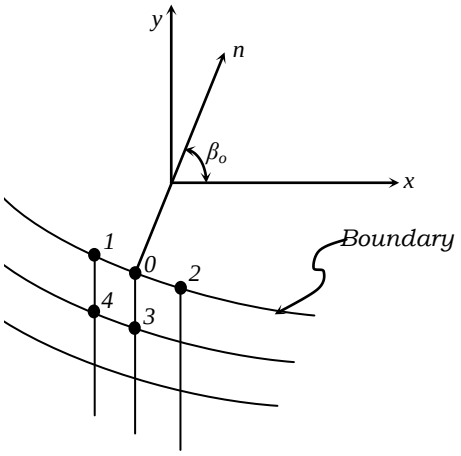

Fig. 9: The Grid Arrangement for the Strip Boundary (Interface) Nodes, Tseng1984

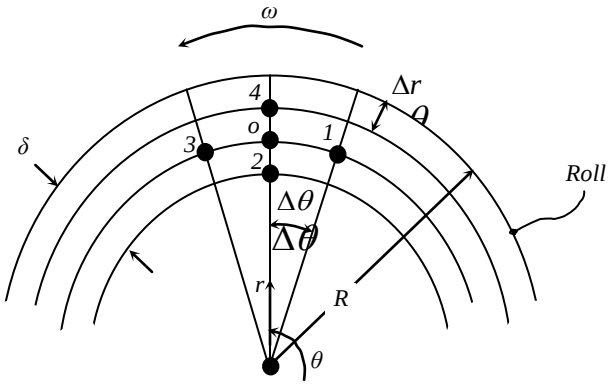

Fig. 10: Neighboring Points Arrangement for Roll Internal Nodes.

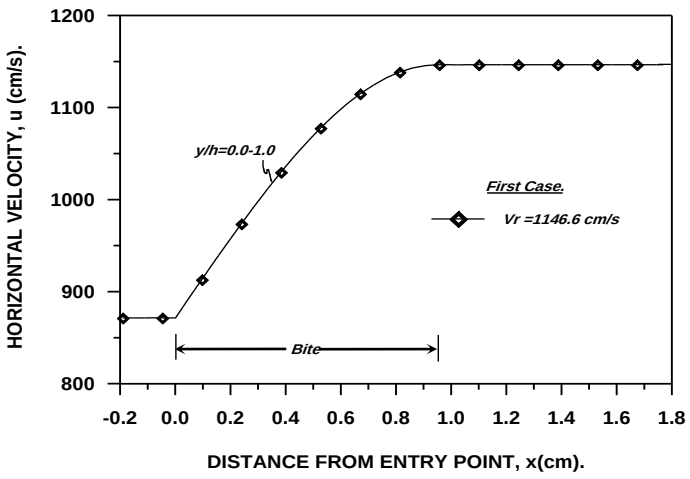

Fig. 11: Horizontal Component of Strip Velocity.

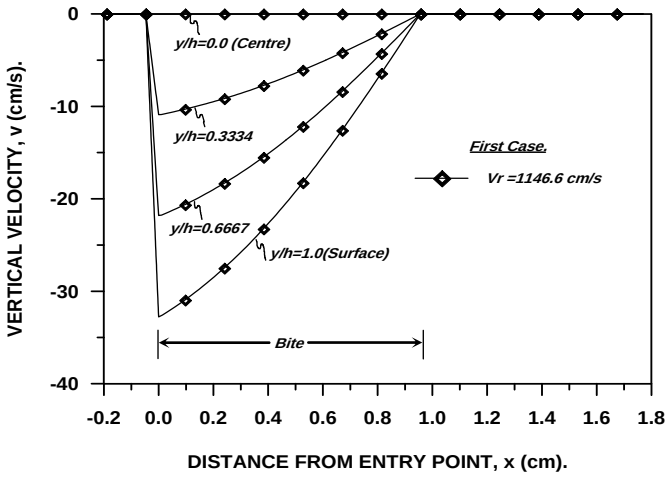

Fig. 12: Vertical Component of Strip Velocity.

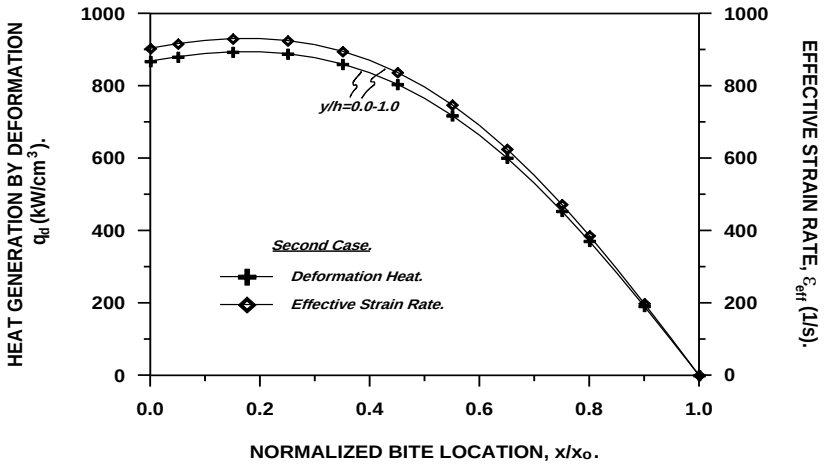

Fig. 13: Effective Strain Rate and Heat Generation by Deformation.

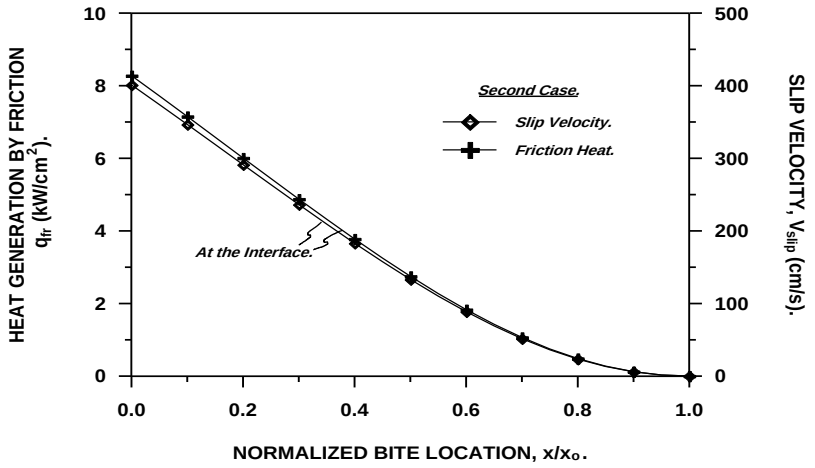

Fig. 14: Slip Velocity and Heat Generation by Friction.

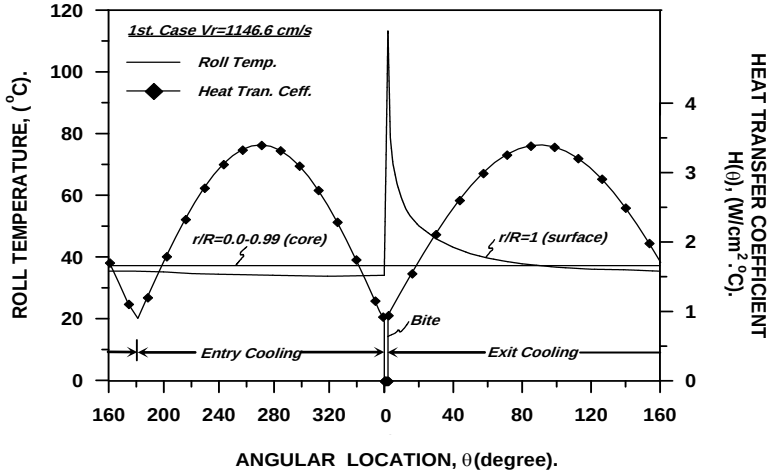

Fig. 15: Heat Transfer Coefficient and Roll Temperature for Cold Rolling Case.

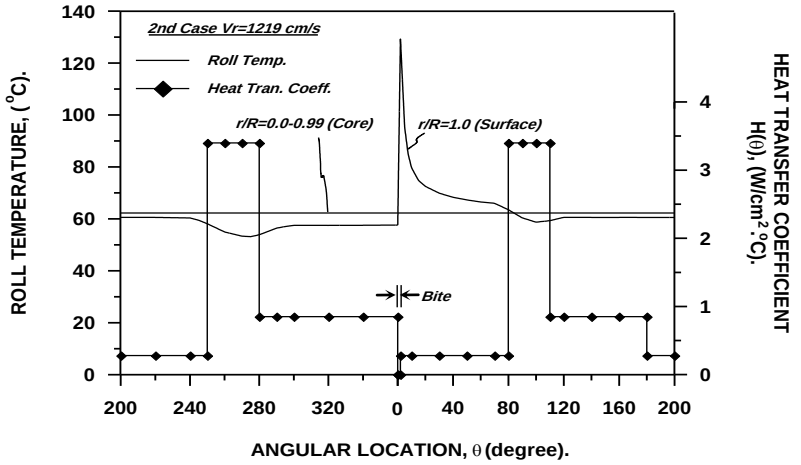

Fig. 16: Heat Transfer Coefficient and Roll Temperature for Cold Rolling Case.

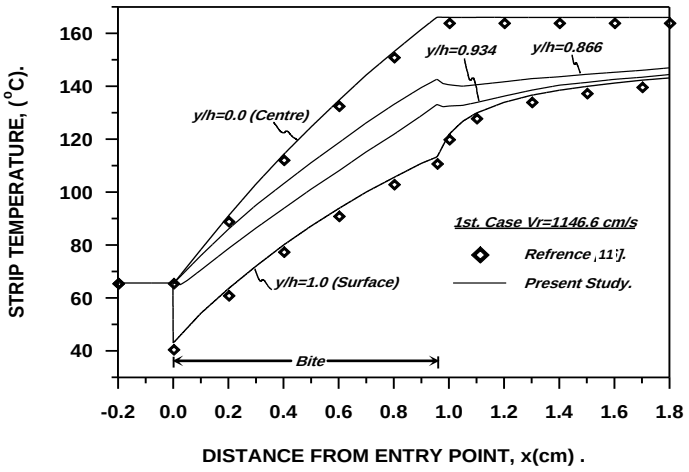

Fig. 17: Comparison of the Strip Temperature for Cold Rolling.

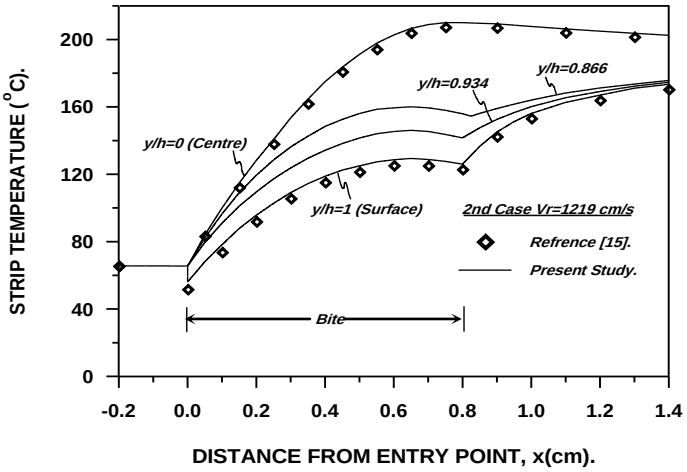

Fig. 18: Comparison of the Strip Temperature for Cold Rolling.

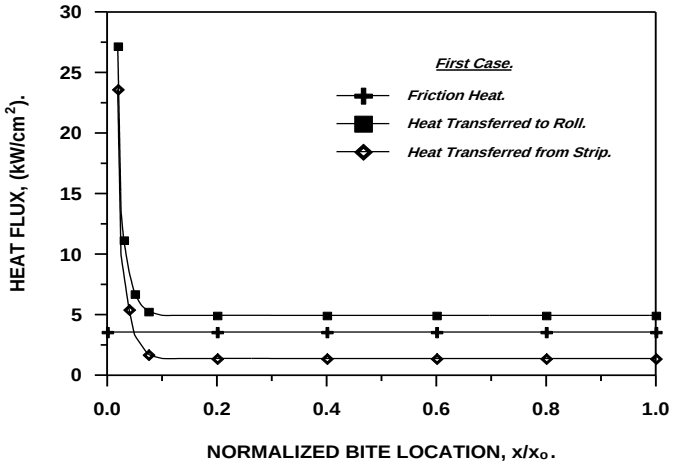

Fig. 19: Distributions of the Interface Heat Flux.

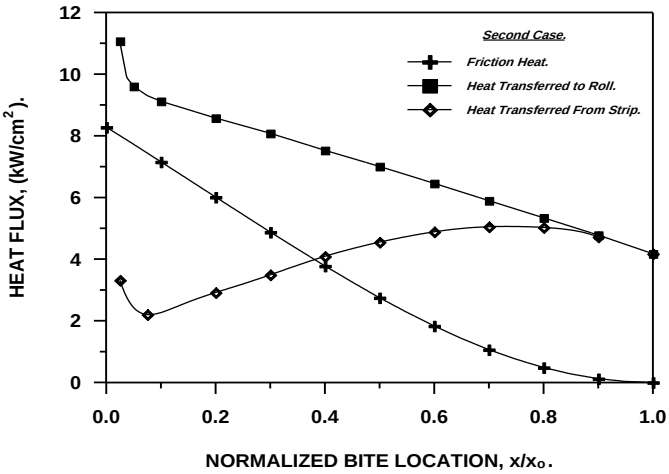

Fig. 20: Distributions of the Interface Heat Flux.

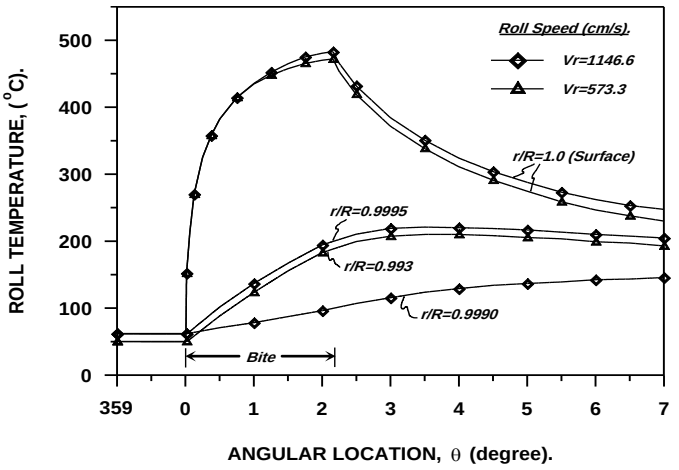

Fig. 21: Roll Temperature near the Bite for Hot Rolling Cases.

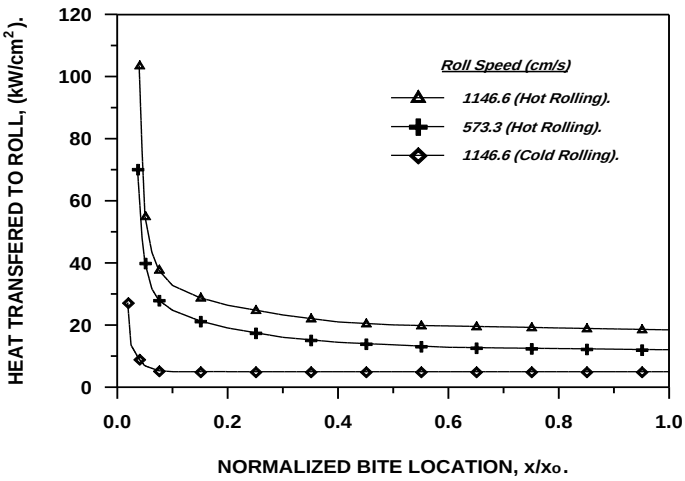

Fig. 22: Distributions of the Interface Heat Flux to Roll.

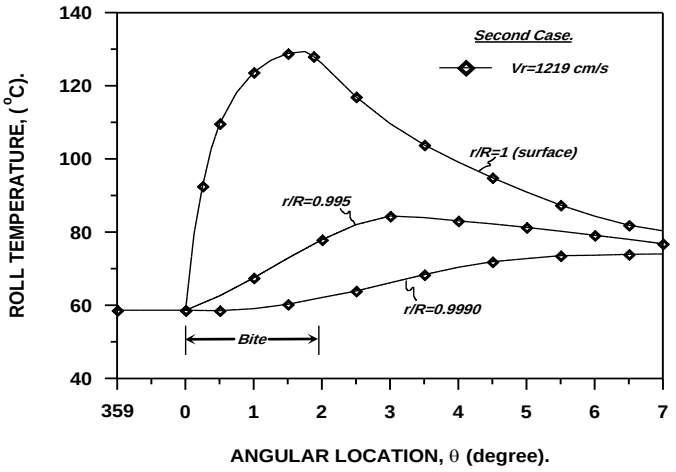

Fig. 23: Roll Temperature near the Bite for Cold Rolling Case.

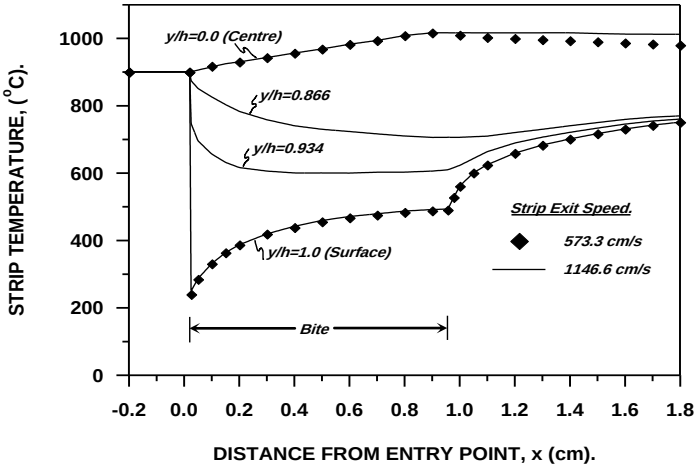

Fig. 24) Strip Temperature for Hot Rolling Cases.

REFERENCES

Bryant, G. F. and Heselton, M. O., "*Roll Gap Temperature Models for Hot Mills*," Metals Technology, 1982, Vol. 9, pp. 469-476.

Bryant, G. F. and Chiu, T. S. L., "*Simplified Roll Temperature Model (Spray Cooling and Stress Effects)*," Metals Technology, 1982, Vol. 9, pp. 485-492.

Chang, D. F., " *An Efficient Way of Calculating Temperatures in the Strip Rolling process*," ASME, Journal of Manufacturing Science and Engineering, 1998, Vol. 120, pp. 93-100.

Dieter, "*Metals Metallurgy*," Mc Graw-George, E-Hill Book, Dieter company, Third addition, 1986.

Johnson, W. and Kudo, H., "*The Use of Upper-Bound Solutions for the Determination of Temperature Distributions in Fast Hot Rolling and Axi-Symmetric Extrusion Process,"* International Journal of Mechanical Science, 1960, Vol. 1, PP. 175-191.

Karagiozis, A. N. and Lenard, J. G., "*Temperature Distribution in A Slab During Hot Rolling*," ASME, Journal of Engineering Materials and Technology, 1988, Vol. 110, pp.17-21.

Lahoti, G. D. and Altan, T., "*Predication of the Temperature Distribution in Axi-Symmetric Compression and Torsion*," ASME, Journal of Engineering Materials and Technology, 1975, Vol. 97, pp.113-120.

Lahoti, G. D., Shah S. N. and Altan, T., "*Computer Aided Heat Transfer Analysis of the Deformation and Temperatures in Strip Rolling*," ASME, Journal of Engineering for Industry, 1978, Vol. 100, pp. 159-166.

Patula, E. T., " *Steady-State Temperature Distribution in A Rotating Roll Subjected to Surface Heat Fluxes and Convective Cooling*," ASME, Journal of Heat Transfer, 1981, Vol. 103, pp. 36-41

Remn-Min Guo, " *Two Dimensional Transient Thermal Behavior of Work Rolls*," ASME, Journal of Manufacturing Science and Technology, 1998, Vol. 120, pp. 28-33.

Sheppard, T. and Wright, D. S., "*Structural and Temperature Variations During Rolling of Aluminum Slabs*," Metals Technology, 1980, Vol. 7, pp. 274-281.

Tseng, A. A., "*A Numerical Heat Transfer Analysis of Strip Rolling*," ASME, Journal of Heat Transfer, 1984, Vol. 106, PP. 512-517.

Tseng, A. A., "*A Generalized Finite Difference Scheme for Convection Dominated Metal Forming Problems*," International Journal for Numerical Methods in Engineering, 1984, Vol.20, pp. 1885-1900.

Tseng, A. A., Tong, S. X., Maslen, S. H. and Mills, J. J., " *Thermal Behavior of Aluminum Rolling*," ASME, Journal of Heat Transfer, 1990, Vol. 112, pp. 301-308.

Zienkiewicz, O. C., Onate, E. and Heinrich, J. C., "*A General Formulation for Coupled Thermal Flow of Metals Using Finite Elements*," International Journal for Numerical Method in Engineering, 1981, Vol. 17, pp. 1497-1514.

NOMENCLATURE

Symbol	***Description***	***Unit***
Bi	Biot Number.	-
c	Specific Heat.	KJ/kg.^{o}C
F	Tangential Force.	N
H	Heat Transfer Coefficient.	W/m^2 .^{o}C.
h	Half Thickness of Strip.	m
k	Thermal Conductivity.	W/m.^{o}C
P	Pressure.	N/m^2
Pe	Peclet Number.	-
Q	Heat Generation.	kW
q	Heat Generation Rate, Heat Friction Rate.	kW/m^3 or

		kW/m^2
R	Roll Radius.	m
r, θ	Cylindrical Coordinate.	-
Re	Reynolds Number.	-
T	Temperature.	^oC
t	Thickness.	m
u, v	Horizontal and Vertical Velocity.	m/s
V	Velocity.	m/s
W	The Width of the Strip.	m
x,y	Cartesian Coordinate.	m

Abbreviations

CFDM	Conventional Finite Difference Method.	-
Coef.	Coefficient.	-
Eq.	Equation.	-
Fig.	Figure.	-
GFDM	Generalized Finite Difference Method.	-
Ref.	Reference.	-
Temp.	Temperature.	^oC
Tran.	Transfer.	-

Greek Symbols

α	Thermal Diffusivity.	m^2/s
ρ	Density.	kg/m^3
ω	Roll Angular Velocity.	rad/s
δ	Heat Penetration Depth.	m
Φ	Bite Angle.	Degree
σ	Plain Strain Yield Stress.	N/m^2
ε	Local Strain Rate.	1/s
β	Angle Specified the Direction.	Degree